ACS Energy Letters

Open Access

http://pubs.acs.org/journal/aelccp

Chalcogen Vacancies Rule Charge Recombination in Pnictogen Chalcohalide Solar-Cell Absorbers

Cibrán López,* Seán R. Kavanagh, Pol Benítez, Edgardo Saucedo, Aron Walsh, David O. Scanlon,* and Claudio Cazorla*

Cite This: *ACS Energy Lett.* 2025, 10, 3562−3569

Read Online

ACCESS | Metrics & More | Article Recommendations | Supporting Information

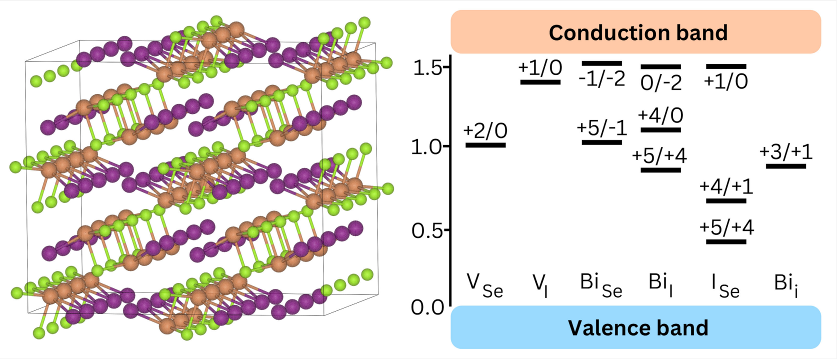

ABSTRACT: **Pnictogen chalcohalides (MChX) represent an emerging class of nontoxic photovoltaic absorbers, valued for their favorable synthesis conditions and optoelectronic properties. Despite their proposed defect tolerance, stemming from the antibonding nature of their valence and conduction bands, their experimentally reported power conversion efficiencies remain below 10%, far from the ideal Shockley−Queisser limit of 30%. Using advanced first-principles simulation methods, we uncover a complex point-defect landscape in MChX, exemplified by BiSeI. Previously overlooked chalcogen vacancies are identified as critical nonradiative charge-recombination centers, which exist in high concentrations and, although they exhibit modest capture coefficients, can reduce the maximum power conversion efficiency down to 24%. We argue that such detrimental effects can be mitigated by cation-poor synthesis conditions and strategic anion substitutions. This study not only identifies efficiency-limiting factors in MChX but also provides a roadmap for their improvement, paving the way for next-generation solution-processed chalcogenide photovoltaics.**

Pnictogen chalcohalides (MChX, M = Bi, Sb; Ch = S, Se; X = I, Br) have garnered significant attention as promising solar-cell absorber materials due to their nontoxicity, low synthesis temperatures (below 300 °C),[1,2] optimal bandgaps ranging from 1.0 to 2.0 eV,[3,4] and exceptional thermodynamic stability.[5,6] Their electron affinities and ionization potentials also align well with established charge transport layers.[7,8] Additionally, their wide bandgap range and high optical absorption coefficients extend their applicability to multijunction solar cell devices, which can potentially exceed the power-conversion efficiencies of conventional single-junction solar cells. These advantageous properties underscore the potential of MChX for next-generation solution-processed solar energy technologies.

Notably, a gap persists between theoretical predictions, which characterize MChX as exceptional photoabsorbers,[9,10] and experimental findings, which report suboptimal MChX photovoltaic performance.[1,7,11] With power conversion efficiencies (PCE) currently below 10%, far from the ideal detailed balance limit of 30%,[12] MChX face significant barriers to commercial viability. This poor PCE is likely due to reduced

Received: April 25, 2025
Revised: June 10, 2025
Accepted: June 20, 2025
Published: June 30, 2025

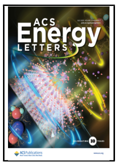

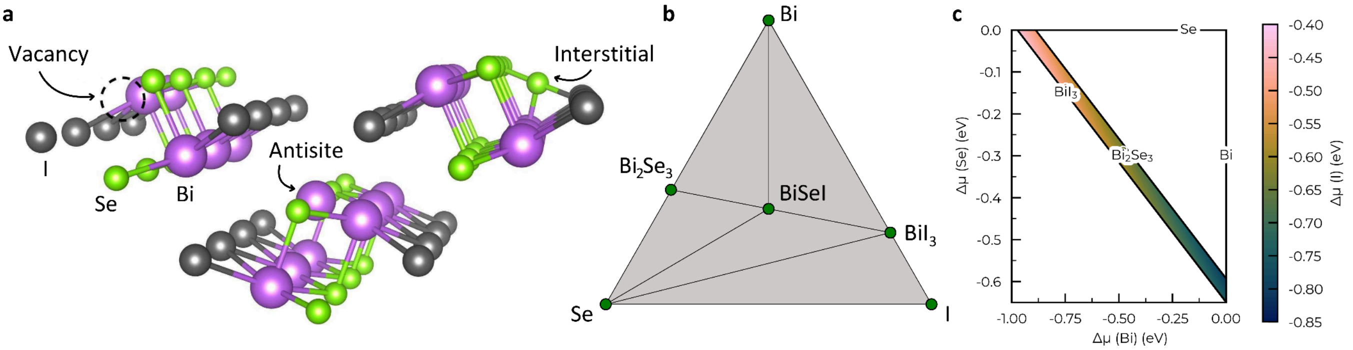

Figure 1. Structural and phase stability properties of BiSeI. a. BiSeI crystal structure (orthorhombic, *Pnma*) characterized by columnar motifs held together by weak van der Waals forces. Point defects considered in this study: vacancies, antisites, and interstitials. Bi, Se and I atoms are represented with purple, green and gray spheres, respectively. b. Convex-hull surface of BiSeI calculated with DFT methods. BiSeI is predicted to be thermodynamically stable against separation into secondary phases because its formation enthalpy is negative relative to the convex-hull surface. c. Chemical stability region, delimited by Se-poor (μ_{Bi}, μ_{Se}, μ_I) = (0, −0.65, −0.75) eV and Bi-poor conditions (μ_{Bi}, μ_{Se}, μ_I) = (−0.97, 0, −0.42) eV (Supplementary Table 1).

carrier lifetimes and nonradiative electron−hole recombination resulting from deep recombination-active defect levels.[13]

MChX semiconductors exhibit antibonding states at the valence band maximum (VBM) and conduction band minimum (CBM), along with high dielectric constants and high charge-carrier mobilities,[14] similar to lead-halide perovskites.[15,16] These features are believed to promote the formation of shallow defect energy levels near the band edges, rather than deep defect levels,[17] indicating potential defect tolerance.[14,18] However, the contrast between this suggested defect tolerance and the observed photovoltaic underperformance suggests the need for a comprehensive investigation of defect chemistry in MChX. This analysis is critical to identify the most detrimental defects and develop effective defect-passivation strategies.[19]

In this study, we present a theoretical investigation of the defect chemistry in MChX, focusing on the representative compound BiSeI. Employing advanced first-principles calculations and defect sampling techniques, we perform a comprehensive analysis of intrinsic point defects, including vacancies, antisites, and interstitials. Among these, Se vacancies (V_{Se}) are identified as the most detrimental defects, significantly undermining photovoltaic efficiency by facilitating nonradiative trap-mediated charge recombination.

Computational Framework. Semiconducting BiSeI crystallizes in an orthorhombic phase (space group *Pnma*) characterized by one-dimensional columns held together by weak van der Waals forces (Figure 1a), closely resembling the structure of pnictogen chalcogenides (e.g., Sb_2Se_3 or Bi_2Se_3[20]). Our density functional theory (DFT) geometry optimizations yield lattice parameters that are in very good agreement with the available experimental data[9] (i.e., a^{DFT} = 4.27 Å, b^{DFT} = 9.04 Å and c^{DFT} = 11.28 Å, to be compared with a^{expt} = 4.22 Å, b^{expt} = 8.70 Å and c^{expt} = 10.58 Å). According to our DFT calculations, BiSeI is thermodynamically stable against phase separation into Bi_2Se_3 and BiI_3 (i.e., $\Delta H = -0.01$ eV/atom referred to the convex hull surface, Figure 1b), with the range of stable chemical potentials for this system given in Figure 1c. These findings are consistent with experimental observations,[1,2] but differ from Materials Project predictions[21] that neglect long-range dispersion forces (Methods).

Crystalline defects can be broadly classified into point and extended defects. Point defects (Figure 1a) include vacancies, where an atom is removed from the lattice (e.g., V_{Se}), antisites, where an atom is replaced by another of a different species (e.g., Bi_{Se}), and interstitials, where an atom occupies a nonequilibrium lattice site (e.g., Se_i). Higher-dimensional defects, such as grain boundaries, dislocations, and precipitates, may also form in materials.[22] However, recent experimental studies indicate that these defects are not prevalent in MChX.[1] Furthermore, chain-like structures are likely to produce grain boundaries that are charge-recombination inactive.[20,23,24] Consequently, this computational work focuses on point defects.

Computational approaches for studying point defects in crystals are well-established, relying on accurate first-principles energy calculations combined with exhaustive exploration of the defect local environment.[25−27] For this work, we employed the supercell approach, which involves modeling point defects within sufficiently large supercells to minimize spurious interactions (Methods). We systematically analyzed all possible vacancy and antisite defects, considering both neutral and charged states. For interstitial defects, we initially evaluated their neutral states by sampling all possible sites obtained from Voronoi analysis (Supplementary Figure 1). Interstitials with sufficiently low formation energies in the neutral state were further analyzed considering multiple charged states. The ShakeNBreak[25,28] defect structure-search approach was employed, revealing numerous significant energy-lowering reconstructions, consistent with observations in similar low-dimensional chalcogenide systems.[29−31]

Spin−orbit coupling (SOC) plays a critical role in shaping the optoelectronic properties of MChX, as well as other well-known classes of functional materials such as hybrid organic−inorganic perovskites (HOIPs). SOC affects the electronic band structure of these compounds by altering the conduction band edge, which is typically derived from heavy elements (e.g., Bi in MChX and Pb in HOIPs).[10,32,33] In MChX, SOC leads to pronounced band gap narrowing and valley splitting, particularly in Bi-based, noncentrosymmetric structures. These effects enhance optical anisotropy but may also reduce carrier mobility.[10,32] In HOIPs, SOC significantly lowers the band gap and can induce Rashba-type spin textures in distorted lattices,

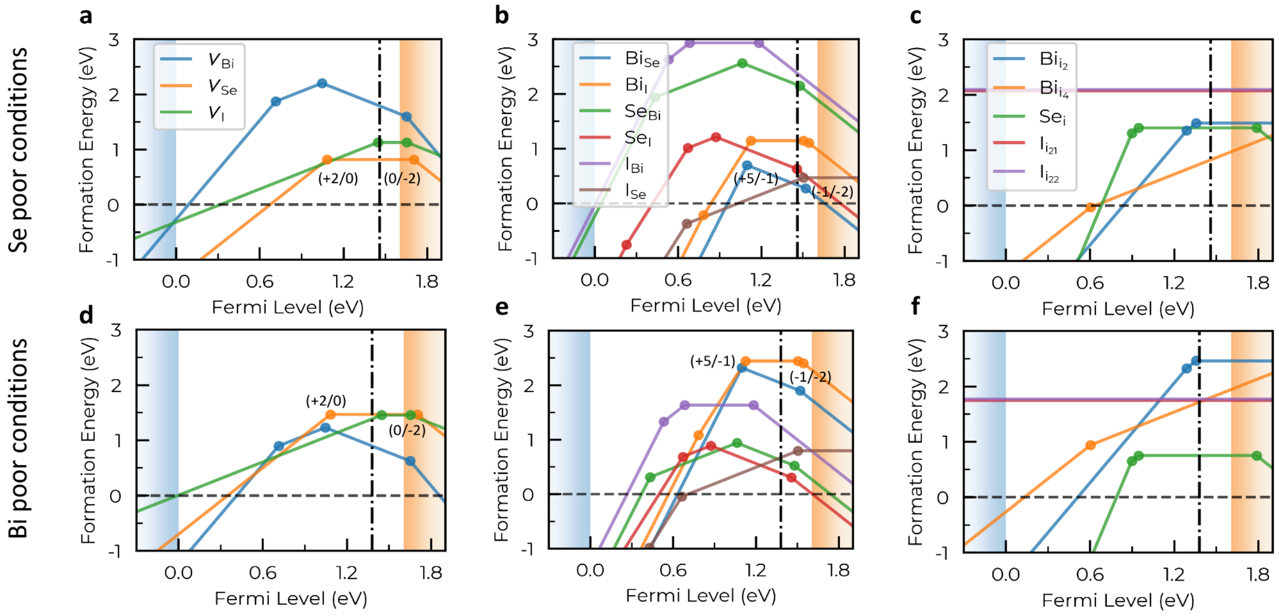

Figure 2. Formation energies of point defects in BiSeI. a−c. Se-poor growth conditions. d−f. Bi-poor growth conditions. The self-consistent Fermi level, E_F^{sc}, is represented with vertical dash-dot lines, lying at 1.46 and 1.38 eV above the VBM (blue shaded region) for Se-poor and Bi-poor growth conditions, respectively (the CBM is represented by the orange shaded region). Numerical subscripts in panels c and f indicate inequivalent lattice interstitial positions (Supplementary Figure 1).

which improves charge separation and radiative lifetimes, both being favorable characteristics for photovoltaic and light-emitting applications.[33] Given these important effects, SOC must be included in *ab initio* simulations of MChX and other optoelectronic materials containing heavy atoms.

First-principles calculations based on DFT[34] were performed using the VASP code[35] (Methods and Supplementary Methods). To address the limitations of semilocal functionals,[36] we employed the range-separated hybrid functional HSEsol,[37,38] which is based on the Perdew−Burke−Ernzerhof exchange-correlation functional revised for solids.[39,40] Long-range dispersion interactions were taken into account through the van der Waals D3 correction scheme.[41] SOC effects, which are particularly relevant for Bi-based MChX,[10,32] were considered in the calculations. All defective atomic structures were fully optimized at the HSEsol+D3+SOC level, a methodology shown to accurately reproduce experimental results for MChX and other similar materials.[9,42] The `doped` simulation package[43] was used to generate defect structures and calculation inputs, determine chemical potential limits, and analyze the defects simulation results.

Defect Formation Energies. Our defect formation energy (E_f) results, expressed as a function of the Fermi level (VBM ≤ E_F ≤ CBM), are shown in Figure 2. These defect formation energies depend on the synthesis conditions (i.e., atomic chemical potentials), defect charge state, and Fermi energy level (Supplementary Methods). A charge-state transition occurs when the energy curves of two different charge states intersect, signaling the potential exchange of charge carriers between the defect and the host material. Defects with low formation energies can significantly impact electron−hole recombination processes, potentially reducing the material's PCE. This effect is particularly detrimental when transition energy levels are deep within the bandgap, as opposed to those near the band edges.[36]

The chemical potentials of BiSeI are bounded by two limiting cases: Se-poor conditions (μ_{Bi}, μ_{Se}, μ_I) = (0, −0.65, −0.75) eV and Bi-poor conditions (μ_{Bi}, μ_{Se}, μ_I) = (−0.97, 0, −0.42) eV (Figure 1c), where the competing secondary phases are Bi−Bi_2Se_3 and Se−BiI_3, respectively. Figure 2 illustrates the E_f results obtained for these two extreme synthesis conditions. Intermediate synthesis conditions can be explored using the open access data provided in[44] and Supplementary Tables 2−7. Regarding experimental synthesis, Se-poor conditions are commonly encountered in physical synthesis routes due to the high volatility of selenium atoms at elevated temperatures.[1,2]

For many defects, the calculated formation energies are very low under Se-poor synthesis conditions (Figure 2a−c), yielding high defect concentrations. Bi-poor conditions, on the other hand, favor moderate to high defect formation energies (Figure 2d−f). Notable examples include: (i) V_{Se}, which exhibits a formation energy of 0.82 eV at the self-consistent Fermi level, E_F^{sc}, under Se-poor conditions compared to 1.47 eV under Bi-poor (Figure 2a,d), and (ii) Bi_{Se}, with E_f = 0.34 eV at E_F^{sc} under Se-poor conditions and 2.04 eV under Bipoor (Figure 2b,e).

In terms of photovoltaic (PV) performance, the most detrimental defects are those with low formation energies at the self-consistent Fermi level.[32] E_F^{sc} is the equilibrium Fermi level that ensures a zero-charge balance across the defect and carrier populations in the system,[45] and it can vary with temperature (e.g., higher temperatures induce larger defect/carrier populations) and chemical potentials (i.e., growth conditions). Therefore, exploration of the self-consistent Fermi level under different temperatures is essential to accurately assess the defects energy and its impact on PV performance.

Under Bi-poor synthesis conditions and at room temperature, E_F^{sc} is positioned 1.38 eV above the VBM (considering defect concentrations generated at a realistic annealing temperature of 550 K). Similarly, under Se-poor growth conditions, E_F^{sc} lies 1.46 eV above the VBM. In both cases, E_F^{sc} exhibits a weak dependence on annealing (Supplementary Figure 2), which indicates a marked *n*-type character for BiSeI.

https://doi.org/10.1021/acsenergylett.5c01267
ACS Energy Lett. 2025, 10, 3562−3569

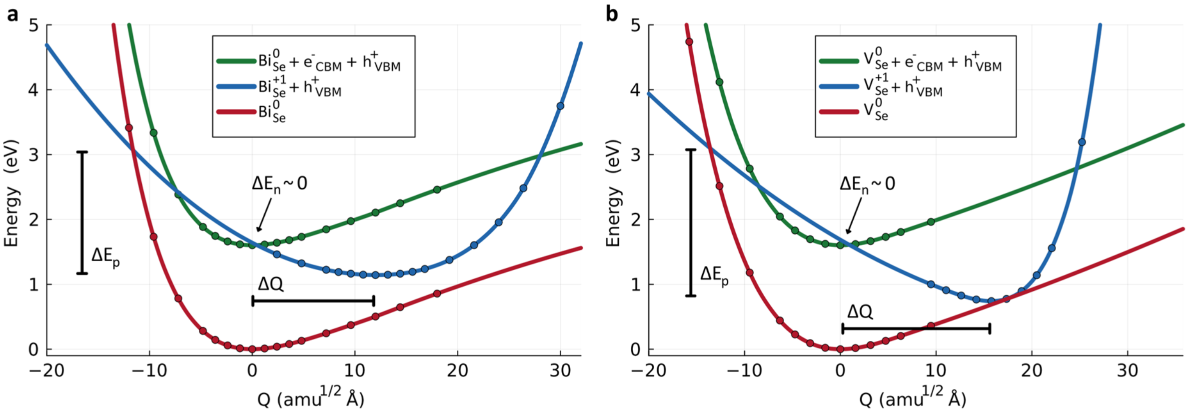

Figure 3. Configuration coordinate diagrams for BiSeI. Configuration coordinate diagrams for a. Bi_{Se} (0/+1) and b. V_{Se} (0/+1). The dots represent potential energies computed from first-principles, and the solid lines are their corresponding quadratic spline interpolation and extrapolation. ΔQ represents the generalized distance between charge states and ΔE_x the electron (n)/hole (p) energy capture barriers.

This behavior is consistent with previous experimental works showing that *p*-type doping is very challenging in MChX.[1]

In Se-poor environments, several antisite defects present very low formation energies at E_F^{sc}, the most critical cases being I_{Se} (0.43 eV) and Bi_{Se} (0.34 eV) (Figure 2b). Bi-poor synthesis conditions generally result in higher formation energies; however, certain antisite defects still exhibit very low E_f (Figure 2e): I_{Se} (0.68 eV), Se_I (0.38 eV), and Se_{Bi} (0.62 eV). Among these, Bi_{Se} stands out as the most detrimental antisite, potentially acting as a *killer* defect under typical experimental synthesis conditions. This defect undergoes a pronounced geometric reconstruction during its (+5/−1) charge-state transition, transforming from a true substitutional defect in the −1 state to a defect complex, $Bi_i + V_{Se}$, in the +5 state (Supplementary Figure 3).

Formation energies of vacancies (Figure 2a,d) and interstitials (Figure 2c,f) commonly are less favorable than those of antisites. The quasi-one-dimensional structure of BiSeI plays a significant role in this E_f trend. Point defects are predominantly confined within the atomic columns where they originate, minimizing interference between neighboring columns (Supplementary Figure 4). Vacancies, which require significant structural adjustments within the affected column, tend to exhibit moderate formation energies. Interstitials, positioned between adjacent columns, are even more challenging to create due to the extensive lattice disruptions that they induce. In contrast, antisite defects, where one atom is replaced by another within the same column, necessitate minimal lattice reorganization and consequently are easier to form. These trends in defect formation are consistent with observations in columnar pnictogen chalcogenides (e.g., Sb_2S_3 and Sb_2Se_3[19,29]).

Among all vacancies, V_{Se} has the lowest formation energy at E_F^{sc}, with a value of 0.82 eV under Se-poor growth conditions. This outcome suggests that V_{Se} could act as a nonradiative charge-recombination center, potentially contributing to PCE losses.

Polaron Formation. Polarons, localized charges accompanied by significant lattice distortions due to strong electron−phonon coupling, can significantly impact carrier recombination via self-trapping mechanisms, potentially limiting PCE.[46] They are generally classified as small or large, depending on their spatial extent and interaction with the lattice. Small polarons are particularly detrimental, as they strongly enhance electron−hole recombination.[47] To assess this possibility, we analyzed carrier self-trapping phenomena induced by defect-bound polarons (Supplementary Discussion). Such processes may be pronounced in BiSeI due to the strong lattice distortions associated with its most critical defects, particularly Bi_{Se}, facilitated by the anharmonic ionic−covalent bonding typical of lone-pair chalcogenides and chalcohalides. However, our calculations reveal weak electron−phonon coupling in BiSeI (Supplementary Discussion), indicating that charge carriers are unlikely to localize via phonon interactions. As a result, polarons in BiSeI are expected to be large, and can reasonably be ruled out as a primary factor limiting the PCE of MChX.

Charge-Carrier Capture Coefficients. Given their low formation energies at the self-consistent Fermi level, V_{Se} and Bi_{Se} are likely the most detrimental defects for PCE among all vacancies and antisites (interstitial defects are not considered further due to their higher E_f values). However, the PV performance of MChX is not solely dictated by defect formation energies. Electron−phonon coupling, particularly its role in electron/hole capture processes that drive non-radiative charge-carrier recombination, may also be critical.[48] To address this aspect, we analyzed the impact of electron−phonon coupling on charge-carrier capture events associated with the V_{Se} (+2/0) and Bi_{Se} (+5/ − 1) charge-state transitions, following the computational methodology introduced in previous studies.[48−50]

In a nutshell, the potential energy surface (PES) of the defect transition is first mapped along the structural path connecting the equilibrium geometries of the two defect charge states involved in the capture process (i.e., the Q coordinate in Figure 3a,b). To accomplish this, multielectron transitions are decomposed into sequential single-electron transition processes, with capture coefficients computed separately for each step [e.g., (+2/+1) and (+1/0) for V_{Se} (+2/0)].[49] Next, from the PES mapping, nuclear wave function overlaps are obtained by solving a one-dimensional Schrödinger equation.[49,50] Electron−phonon coupling is then evaluated using static perturbation theory. Finally, combining these results with phonon overlaps and scaling factors that account for charge interaction effects, the carrier capture coefficients are determined[48] (Supplementary Methods).

For both V_{Se} and Bi_{Se} charge-state transitions, the most detrimental single-electron capture process for PV performance occurs at the (0/+1) level, as it exhibits the highest electron/hole capture coefficients ($C_{n/p}$, Supplementary Table 8). Therefore, we focus on this particular process here. Since the estimated $C_{n/p}$ coefficients show minimal temperature dependence (Supplementary Figure 5), we neglect this effect in the following discussion.

The energy barriers for (0/+1) electron and hole capture processes, $\Delta E_{n/p}$, are critical parameters in determining $C_{n/p}$ (Supplementary Methods). In BiSeI, the electron capture barriers (ΔE_n, Figure 3) are found to be nearly negligible for both V_{Se} and Bi_{Se}. In contrast, the hole capture barriers (ΔE_p, Figure 3) are significant, amounting to 2.36 and 1.93 eV for V_{Se} and Bi_{Se}, respectively. These $\Delta E_{n/p}$ results suggest high C_n and low C_p for MChX.

Although this expectation holds for Bi_{Se} ($C_n = 6.20 \times 10^{-11}$ cm^3/s and $C_p < 10^{-20}$ cm^3/s), it does not hold for V_{Se}. Specifically, the room-temperature hole capture coefficient estimated for V_{Se} is notably high, reaching 9.85×10^{-8} cm^3/s, while its electron capture coefficient is 1.91×10^{-10} cm^3/s (Supplementary Figure 5 and Supplementary Table 8). This unexpected result stems from factors beyond $\Delta E_{n/p}$, such as electron−phonon coupling and phonon wave function overlaps, which also play a critical role in carrier capture processes (Supplementary Methods).

The capture coefficient values estimated for BiSeI are relatively small compared to those found in similar materials such as Sb_2Se_3 ($C_n = 5.63 \times 10^{-6}$ cm^3/s and $C_p = 1.22 \times 10^{-8}$ cm^3/s).[51] At first glance, this comparison suggests that defect chemistry may have a notable, though less pronounced, impact on the PV efficiency of BiSeI compared to Sb_2Se_3. However, as we will discuss in the next section, this expectation does not hold.

Power Conversion Efficiency and Defect Mitigation Strategies. The detailed balance model,[12] which neglects nonradiative charge-carrier recombination losses, predicts a maximum PCE of 30.47% for BiSeI at room temperature, along with an open-circuit voltage (V_{oc}) of 1.33 V and a fill factor (FF) of 90.54%.[9] This ideal Shockley−Queisser limit assumes that each absorbed photon generates an electron−hole pair and that all charge-carrier recombination is purely radiative. When thickness-dependent absorptivity is considered, the radiative efficiency limit for a 700 nm-thick absorber layer slightly decreases to 30.39%, accompanied by a reduced V_{oc} of 1.33 V and a nearly unchanged FF of 90.54%. These results underscore the potential of BiSeI for photovoltaic applications, as its power conversion efficiency is only minimally affected by finite-layer thickness. However, as noted earlier, PV cells based on MChX absorbers have yet to exceed a PCE of 10%.[1,7,11] While factors such as material morphology and device architecture may contribute to this limitation, our findings suggest that trap-mediated nonradiative charge recombination could also play a significant role in reducing PV efficiency.

The maximum defect-limited PCE of BiSeI, η, can be estimated using the calculated $C_{n/p}$, defect concentrations, and related parameters (Supplementary Methods).[52] Under Se-poor synthesis conditions and assuming an annealing temperature of 550 K, we estimate η = 24.2%, a notable reduction of over 6% compared to the ideal detailed balance limit. Separate η calculations for Bi_{Se} and V_{Se} defects reveal that this efficiency loss originates entirely from the selenium vacancy. In fact, the maximum PCE estimated when considering only the antisite defect remains nearly identical to the ideal limit, owing to its extremely low carrier capture coefficients. Therefore, substitutional traps such as Bi_{Se}, and similarly I_{Se} (Figure 2b,e), can be regarded as electronically benign and ruled out as significant nonradiative recombination centers in BiSeI.

The nonradiative efficiency loss in BiSeI is comparable to that observed in other light absorber materials, such as Cu_2ZnSnS_4,[53] $Cu_2ZnSnSe_4$,[48] and CdTe.[54] Additionally, the PCE loss in BiSeI is accompanied by a notable reduction in open-circuit voltage (V_{oc} = 1.08 V) and fill factor (FF = 88.81%), indicating a deterioration in electronic quality under illumination and reduced charge transport efficiency.

The η estimated for BiSeI is slightly lower than that of Sb_2Se_3, which has a predicted defect-limited efficiency of 26%.[51] At first glance, this result may seem counterintuitive, as the calculated carrier capture coefficients for Sb_2Se_3 are significantly higher than those for BiSeI. However, the discrepancy is explained by the lower defect formation energies in BiSeI (e.g., 1.2 eV for V_{Se} in Sb_2Se_3[51] versus 0.8 eV for the same defect in BiSeI), which lead to a substantially higher concentration of defects and free carriers (Figure 4a). This finding highlights that PCE limitations in MChX semiconductors arise primarily from the high abundance of defects, rather than their individual recombination strengths. As a result, effective defect passivation strategies could play a critical role in improving the PV performance of these materials.

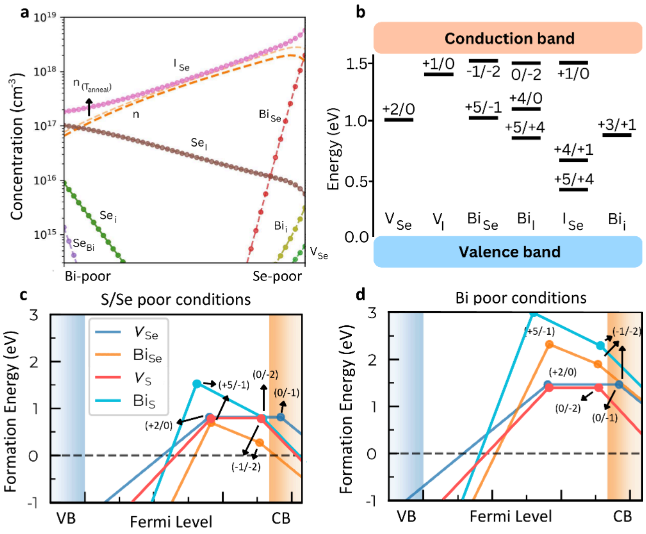

Figure 4. Point defect chemistry of BiSeI and BiSBr. a. Defect concentrations of BiSeI considering an annealing temperature of 550 K. b. Sketch of the most prominent (i.e., lowest energy) point defects determined for BiSeI. Defect formation energies for BiSeI and BiSBr evaluated under c. S/Se-poor and d. Bi-poor growth conditions. The formation energy of Bi_S is significantly higher than that of Bi_{Se}.

Based on our first-principles computational results, several strategies can be proposed to mitigate the formation of PV-detrimental defects in MChX. One promising approach is optimizing synthesis conditions. In particular, our study demonstrates that adopting Bi-poor growth conditions, despite the associated practical challenges,[1] significantly increases the formation energy of most defects (Figure 2), thereby reducing their prevalence. Notably, under Bi-poor synthesis conditions, our calculated η reaches 30.39%, remaining very close to the ideal detailed balance limit, with an open-circuit voltage of 1.33 V and a fill factor of 90.54%.

Another approach to mitigating PCE losses is ion substitution, which provides a practical and controlled method for engineering defect chemistry (Figure 4b). The similar ionic radii of Bi (r_{Bi} = 207 pm), Se (r_{Se} = 190 pm), and I (r_{I} = 198 pm) facilitate their interchangeability and diffusion at elevated temperatures, promoting the formation of antisite and vacancy defects. To address this issue, we propose chemically guided ion substitutions involving atomic species with larger ionic radius differences, while preserving the desirable optoelectronic properties. Based on this principle, BiSBr emerges as a promising MChX candidate for reduced defect concentrations, benefiting from the substantial size mismatch among Bi (r_{Bi} = 207 pm), S (r_{S} = 180 pm), and Br (r_{Br} = 183 pm).

Supplementary defect calculations confirm that some defects in BiSeI can be significantly passivated through compositional substitution in BiSBr (Figure 4c,d). Specifically, under S-poor synthesis conditions, the charge-state transition $\mathrm{Bi_S}$ $(-1/-2)$ exhibits a formation energy of 0.80 eV, compared to only 0.28 eV for $\mathrm{Bi_{Se}}$ in BiSeI (Figure 4c). Similarly, under Bi-poor conditions, the formation energy of $\mathrm{Bi_S}$ $(-1/-2)$ increases to 2.30 eV, while that of $\mathrm{Bi_{Se}}$ remains lower at 1.90 eV (Figure 4d). In contrast, the formation energy of sulfur and selenium vacancy charge-state transitions remain nearly unchanged across the two compounds, with Bi-poor conditions being generally the most favorable for defect suppression (Figure 4c,d). Overall, the Se→S and I→Br substitutions preserve the charge-state transition levels of vacancy defects, while increasing the formation energies of antisite defects by more than 200%. This substantial enhancement contributes to the improved defect tolerance of BiSBr compared to BiSeI.

Finally, it is hypothesized that additional ion substitutions could further enhance defect mitigation in MChX materials[55] by reducing antisite and vacancy concentrations. For instance, BiOI, which exhibits a significant size difference between O (r_{O} = 152 pm) and I (r_{I} = 198 pm), presents a Bi−O ionic radius difference of 55 pm, that is, more than 220% larger than the Bi−Se difference in BiSeI. Similarly, the I−O ionic radius difference of 46 pm represents a 475% increase compared to the I−Se difference in BiSeI. Notably, BiOI has recently emerged as a promising candidate for both photocatalysis[56] and photovoltaic absorption,[57,58] suggesting that it may exhibit great defect tolerance in addition to excellent optoelectronic properties.

In conclusion, this study identifies the critical role of point defects in limiting the PV performance of MChX light absorbers, with BiSeI as model system. Using advanced first-principles and configuration sampling methods, we show that V_{Se}, followed by $\mathrm{Bi_{Se}}$, is the most detrimental defect, significantly facilitating nonradiative charge-carrier recombination. These defects reduce the maximum PCE of BiSeI down to approximately 24%, which is about 6% smaller than the corresponding ideal detailed balance limit. This performance loss is accompanied by reductions in open-circuit voltage (V_{oc} = 1.08 V) and fill factor (FF = 88.81%). Nevertheless, we propose potential defect mitigation strategies based on synthesis conditions and chemical substitutions. Specifically, Bi-poor growth conditions significantly increase the formation energies of V_{Se} and $\mathrm{Bi_{Se}}$, reducing their concentrations. Additionally, the ion substitutions S→Se and Br→I offer promising improvements in defect tolerance.

The findings presented in this study are significant for the field of photovoltaics, as they provide a pathway to enhance the efficiency of MChX light absorbers, a promising class of nontoxic and thermodynamically stable materials. By addressing defect chemistry and proposing effective passivation strategies, this study not only bridges the gap between theoretical predictions and experimental performance but also establishes a framework for designing more efficient solar absorbers with improved defect tolerance. These insights could pave the way for next-generation photovoltaic technologies with higher efficiencies and broader applicability.

Methods. *Ab initio* calculations based on density functional theory (DFT) were performed to analyze point defects in MChX. These calculations were conducted with the `VASP` software package[35] using the generalized gradient approximation to the exchange-correlation energy for solids due to Perdew et al. (PBEsol).[39] Since MChX are van der Waals materials, long-range dispersion interactions were taken into account through the D3 scheme.[41] The projector augmented-wave method was used to represent the ionic cores[59] and for each element the maximum possible number of valence electronic states was considered. Wave functions were represented in a plane-wave basis typically truncated at 600 eV. By using these parameters and a dense **k**-point grid for reciprocal space Brillouin zone integration of 11 × 5 × 4 (centered at Γ), the resulting energies were converged to within 1 meV per formula unit. In the geometry relaxations, a tolerance of 0.5 $\mathrm{meV \cdot Å^{-1}}$ was imposed in the atomic forces. Defect calculations were performed in 3 × 2 × 1 (12.8 × 18.1 × 11.3 Å) supercells, using a 2 × 1 × 2 Γ-centered **k**-point grid. For the estimation of optoelectronic properties (e.g., band gaps and optical absorption coefficients), spin−orbit coupling corrections were taken into account along with range-separated hybrid functionals containing an exact Hartree−Fock exchange fraction of 25% (i.e., HSEsol+SOC[37,38,40]). Additional details of our defects formation energy and capture coefficients DFT calculations can be found in the Supplementary Methods.

■ ASSOCIATED CONTENT

Data Availability Statement

The data that support the findings of this study, comprising the single-point energy and local potential calculations for all relaxed defects, have been made publicly available.[44]

Supporting Information

The Supporting Information is available free of charge at https://pubs.acs.org/doi/10.1021/acsenergylett.5c01267.

Additional figures, tables, details of the DFT calculations and a discussion, as mentioned in the text (PDF)

■ AUTHOR INFORMATION

Corresponding Authors

Cibrán López − *Departament de Física, Universitat Politècnica de Catalunya, 08034 Barcelona, Spain; Barcelona Research Center in Multiscale Science and Engineering, Universitat Politècnica de Catalunya, 08019 Barcelona, Spain*; Email: cibran.lopez@upc.edu

David O. Scanlon − *School of Chemistry, University of Birmingham, Birmingham B15 2TT, U.K.*; orcid.org/0000-0001-9174-8601; Email: d.o.scanlon@bham.ac.uk

Claudio Cazorla − *Departament de Física, Universitat Politècnica de Catalunya, 08034 Barcelona, Spain; Barcelona Research Center in Multiscale Science and Engineering, Universitat Politècnica de Catalunya, 08019 Barcelona, Spain*; orcid.org/0000-0002-6501-4513; Email: claudio.cazorla@upc.edu

Authors

Seán R. Kavanagh − *Harvard University Center for the Environment, Cambridge, Massachusetts 02138, United States;* orcid.org/0000-0003-4577-9647

Pol Benítez − *Departament de Física, Universitat Politècnica de Catalunya, 08034 Barcelona, Spain; Barcelona Research Center in Multiscale Science and Engineering, Universitat Politècnica de Catalunya, 08019 Barcelona, Spain*

Edgardo Saucedo − *Barcelona Research Center in Multiscale Science and Engineering, Universitat Politècnica de Catalunya, 08019 Barcelona, Spain; Department of Electronic Engineering, Universitat Politècnica de Catalunya, 08034 Barcelona, Spain*

Aron Walsh − *Thomas Young Centre and Department of Materials, Imperial College London, London SW7 2AZ, U.K.; Department of Physics, Ewha Womans University, Seoul 03760, South Korea;* orcid.org/0000-0001-5460-7033

Complete contact information is available at:
https://pubs.acs.org/10.1021/acsenergylett.5c01267

Author Contributions

C.L., E.S., and C.C. conceived the study and planned the research, which was discussed in-depth with the rest of the co-authors. C.L., S.K., and P.B. performed the first-principles calculations and analyzed the results. The manuscript was written by C.L. and C.C., with substantial input from the rest of the co-authors.

Notes

The authors declare no competing financial interest.

■ ACKNOWLEDGMENTS

C.L. acknowledges support from the Spanish Ministry of Science, Innovation and Universities under a FPU grant. S.R.K. acknowledges the Harvard University Center for the Environment (HUCE) for funding a fellowship. C.C. acknowledges support by MICIN/AEI/10.13039/501100011033 and ERDF/EU under the grants TED2021-130265B-C22, TED2021-130265B-C21, PID2023-146623NB-I00, PID2023-147469NB-C21 and RYC2018-024947-I and by the Generalitat de Catalunya under the grants 2021SGR-00343, 2021SGR-01519 and 2021SGR-01411. Computational support was provided by the Red Española de Supercomputación under the grants FI-2024-1-0005, FI-2024-2-0003 and FI-2024-3-0004. This work is part of the Maria de Maeztu Units of Excellence Programme CEX2023-001300-M funded by MCIN/AEI (10.13039/501100011033). P.B. acknowledges support from the predoctoral program AGAUR-FI ajuts (2024 FI-1 00070) Joan Oró. E.S. acknowledge the European Union H2020 Framework Program SENSATE project: Low dimensional semiconductors for optically tunable solar harvesters (grant agreement Number 866018), Renew-PV European COST action (CA21148), the Spanish Ministry of Science and Innovation ACT-FAST (PCI2023-145971-2), and the ICREA Academia Program.

■ REFERENCES

(1) Caño, I.; Navarro-Güell, A.; Maggi, E.; Barrio, M.; Tamarit, J.-L.; Svatek, S.; Antolín, E.; Yan, S.; Barrena, E.; Galiana, B.; Placidi, M.; Puigdollers, J.; Saucedo, E. SbSeI and SbSeBr micro-columnar solar cells by a novel high pressure-based synthesis process. *J. Mater. Chem. A* **2023**, *11*, 17616−17627.

(2) Li, S.; Huang, Z.; Ding, Y.; Zhang, C.; Yu, J.; Feng, Q.; Feng, J. Growth of BiSBr microsheet arrays for enhanced photovoltaics performance. *Small* **2024**, *20*, 2306964.

(3) Ghorpade, U. V.; Suryawanshi, M. P.; Green, M. A.; Wu, T.; Hao, X.; Ryan, K. M. Emerging chalcohalide materials for energy applications. *Chem. Rev.* **2023**, *123*, 327.

(4) He, J.; Hu, X.; Liu, Z.; Chen, W.; Longo, G. Prospect for bismuth/antimony chalcohalides-based solar cells. *Adv. Funct. Mater.* **2023**, *33*, 2306075.

(5) Nie, R.; Im, J.; Seok, S. I. Efficient solar cells em- ploying light-harvesting $Sb_{0.67}Bi_{0.33}SI$. *Adv. Mater.* **2019**, *31*, 1808344.

(6) Li, Y.; Wang, S.; Hong, J.; Zhang, N.; Wei, X.; Zhu, T.; Zhang, Y.; Xu, Z.; Liu, K.; Jiang, M.; Xu, H. Polarization-sensitive photodetector based on high crystallinity quasi-1d BiSeI nanowires synthesized via chemical vapor deposition. *Small* **2023**, *19*, 2302623.

(7) Tiwari, D.; Cardoso-Delgado, F.; Alibhai, D.; Mombrú, M.; Fermín, D. J. Photovoltaic performance of phase-pure orthorhombic BiSI thin-films. *ACS Appl. Energy Mater.* **2019**, *2*, 3878−3885.

(8) Guo, X.; Huang, Y.-T; Lohan, H.; et al. Air-stable bis- muth sulfobromide (BiSBr) visible-light absorbers: opto- electronic properties and potential for energy harvesting. *J. Mater. Chem. A* **2023**, *11*, 22775.

(9) López, C.; Caño, I.; Rovira, D.; Benítez, P.; Asensi, J. M.; Jehl, Z.; Tamarit, J.-L.; Saucedo, E.; Cazorla, C. Machine-learning aided first-principles prediction of earth-abundant pnictogen chalcohalide solid solutions for solar-cell devices. *Adv. Funct. Mater.* **2024**, *34*, 2406678.

(10) Ganose, A. M.; Butler, K. T.; Walsh, A.; Scanlon, D. O. Relativistic electronic structure and band alignment of BiSI and BiSeI: candidate photovoltaic materials. *J. Mater. Chem. A* **2016**, *4*, 2060−2068.

(11) Nie, R.; Hu, M.; Risqi, A. M.; Li, Z.; Seok, S. I. Efficient and stable antimony selenoiodide solar cells. *Adv. Sci.* **2021**, *8*, 2003172.

(12) Shockley, W.; Queisser, H. J. Detailed balance limit of efficiency of p−n junction solar cells. *J. Appl. Phys.* **1961**, *32*, 510−519.

(13) Kavanagh, S. R.; Nielsen, R. S.; Hansen, J. L.; Davidsen, R. S.; Hansen, O.; Samli, A. E.; Vesborg, P. C. K.; Scanlon, D. O.; Walsh, A. Intrinsic point defect tolerance in selenium for indoor and tandem photovoltaics. *Energy Environ. Sci.* **2025**, *18*, 4431−4446.

(14) Ran, Z.; Wang, X.; Li, Y.; et al. Bismuth and antimony-based oxyhalides and chalcohalides as potential optoelectronic materials. *npj Comput. Mater.* **2018**, *4*, 14.

(15) Walsh, A.; Zunger, A. Instilling defect tolerance in new compounds. *Nat. Mater.* **2017**, *16*, 964−967.

(16) Huang, Y.-T.; Kavanagh, S. R.; Scanlon, D. O.; Walsh, A.; Hoye, R. L. Z. Perovskite-inspired materials for photovoltaics and beyond—from design to devices. *Nanotechnology* **2021**, *32*, 132004.

(17) Zakutayev, A.; Caskey, C. M.; Fioretti, A. N.; Ginley, D. S.; Vidal, J.; Stevanovic, V.; Tea, E.; Lany, S. Defect tolerant semiconductors for solar energy conversion. *J. Phys. Chem. Lett.* **2014**, *5*, 1117−1125.

(18) Zhang, S. B.; Wei, S.-H.; Zunger, A.; Katayama-Yoshida, H. Defect physics of the $CuInSe_2$ chalcopyrite semiconductor. *Phys. Rev. B* **1998**, *57*, 9642−9656.

(19) Savory, C. N.; Scanlon, D. O. The complex defect chemistry of antimony selenide. *J. Mater. Chem. A* **2019**, *7*, 10739−10744.

(20) Zhou, Y.; Wang, L.; Chen, S.; et al. Thin-film Sb_2Se_3 photovoltaics with oriented one-dimensional ribbons and benign grain boundaries. *Nat. Photonics* **2015**, *9*, 409−415.

(21) Jain, A.; Ong, S. P.; Hautier, G.; Chen, W.; Richards, W. D.; Dacek, S.; Cholia, S.; Gunter, D.; Skinner, D.; Ceder, G.; Persson, K. A. Commentary: The materials project: A materials genome approach to accelerating materials innovation. *APL Mater.* **2013**, *1*, No. 011002.

(22) Ball, J. M.; Petrozza, A. Defects in perovskite-halides and their effects in solar cells. *Nature Energy* **2016**, *1*, 16149.

(23) McKenna, K. P. Self-healing of broken bonds and deep gap states in Sb_2Se_3 and Sb_2S_3. *Adv. Electron. Mater.* **2021**, *7*, 2000908.

(24) Williams, R. E.; Ramasse, Q. M.; McKenna, K. P.; Phillips, L. J.; Yates, P. J.; Hutter, O. S.; Durose, K.; Major, J. D.; Mendis, B. G.

Evidence for self-healing benign grain boundaries and a highly defective Sb_2Se_3-CdS interfacial layer in Sb_2Se_3 thin-film photovoltaics. *ACS Appl. Mater. Interfaces* **2020**, *12*, 21730−21738.

(25) Mosquera-Lois, I.; Kavanagh, S. R.; Walsh, A.; Scanlon, D. O. Shakenbreak: Navigating the defect configurational landscape. *JOSS* **2022**, *7*, 4817.

(26) Freysoldt, C.; Neugebauer, J.; Van de Walle, C. G. Fully ab initio finite-size corrections for charged-defect supercell calculations. *Phys. Rev. Lett.* **2009**, *102*, No. 016402.

(27) Kumagai, Y.; Oba, F. Electrostatics-based finite-size corrections for first-principles point defect calculations. *Phys. Rev. B* **2014**, *89*, 195205.

(28) Mosquera-Lois, I.; Kavanagh, S. R. In search of hidden defects. *Matter* **2021**, *4* (8), 2602−2605.

(29) Wang, X.; Kavanagh, S. R.; Scanlon, D. O.; Walsh, A. Four-electron negative-*u* vacancy defects in antimony selenide. *Phys. Rev. B* **2023**, *108*, 134102.

(30) Wang, X.; Kavanagh, S. R.; Walsh, A. Sulfur vacancies limit the open-circuit voltage of Sb_2S_3 solar cells. *ACS Energy Lett.* **2025**, *10*, 161−167.

(31) Mosquera-Lois, I.; Kavanagh, S. R.; Ganose, A. M.; Walsh, A. Machine-learning structural reconstructions for accelerated point defect calculations. *npj Computational Materials* **2024**, *10* (1), 121.

(32) Ganose, A. M.; Matsumoto, S.; Buckeridge, J.; Scanlon, D. O. Defect engineering of earth-abundant solar absorbers BiSI and BiSeI. *Chem. Mater.* **2018**, *30*, 3827−3835.

(33) Anandan, P. R.; Nadeem, M.; Lin, C.-H.; Singh, S.; Guan, X.; Kim, J.; Shahrokhi, S.; Rahaman, M. Z.; Geng, X.; Huang, J.-K.; Nguyen, H.; Hu, H.; Sharma, P.; Seidel, J.; Wang, X.; Wu, T. Spin−orbital coupling in all-inorganic metal-halide perovskites: The hidden force that matters. *Applied. Physics Reviews* **2023**, *10* (4), No. 041312.

(34) Cazorla, C.; Boronat, J. Simulation and understanding of atomic and molecular quantum crystals. *Rev. Mod. Phys.* **2017**, *89*, No. 035003.

(35) Kresse, G.; Furthmüller, J. Efficient iterative schemes for *ab initio* total-energy calculations using a plane-wave basis set. *Phys. Rev. B* **1996**, *54*, 11169.

(36) Freysoldt, C.; Grabowski, B.; Hickel, T.; Neugebauer, J.; Kresse, G.; Janotti, A.; Van de Walle, C. G. First-principles calculations for point defects in solids. *Rev. Mod. Phys.* **2014**, *86*, 253−305.

(37) Heyd, J.; Scuseria, G. E.; Ernzerhof, M. Hybrid functionals based on a screened coulomb potential. *J. Chem. Phys.* **2003**, *118*, 8207−8215.

(38) Krukau, A. V.; Vydrov, O. A.; Izmaylov, A. F.; Scuseria, G. E. Influence of the exchange screening parameter on the performance of screened hybrid functionals. *J. Chem. Phys.* **2006**, *125*, 224106.

(39) Perdew, J. P.; Ruzsinszky, A.; Csonka, G. I.; Vydrov, O. A.; Scuseria, G. E.; Constantin, L. A.; Zhou, X.; Burke, K. Restoring the density-gradient expansion for exchange in solids and surfaces. *Phys. Rev. Lett.* **2008**, *100*, 136406.

(40) Schimka, L.; Harl, J.; Kresse, G. Improved hybrid functional for solids: The hsesol functional. *J. Chem. Phys.* **2011**, *134*, No. 024116.

(41) Grimme, S.; Antony, J.; Ehrlich, S.; Krieg, S. A consistent and accurate *ab initio* parametrization of density functional dispersion correction (dft-d) for the 94 elements H-Pu. *J. Chem. Phys.* **2010**, *132*, 154104.

(42) Pan, J.; Metzger, W. K.; Lany, S. Spin-orbit coupling effects on predicting defect properties with hybrid functionals: A case study in CdTe. *Phys. Rev. B* **2018**, *98*, No. 054108.

(43) Kavanagh, S. R.; Squires, A. G.; Nicolson, A.; Mosquera-Lois, I.; Ganose, A. M.; Zhu, B.; Brlec, K.; Walsh, A.; Scanlon, D. O. doped: Python toolkit for robust and repeatable charged defect supercell calculations. *Journal of Open Source Software* **2024**, *9*, 6433.

(44) López, C.; Cazorla, C. BiSeI intrinsic point defects. *NOMAD*, 2025. https://dx.doi.org/10.17172/NOMAD/2024.06.29-1.

(45) Squires, A. G.; Scanlon, D. O.; Morgan, B. J. py-sc-fermi: self-consistent fermi energies and defect concentrations from electronic structure calculations. *JOSS* **2023**, *8*, 4962.

(46) Kavanagh, S. R.; Savory, C. N.; Scanlon, D. O.; Walsh, A. Hidden spontaneous polarisation in the chalcohalide photovoltaic absorber $Sn_2SbS_2I_3$. *Mater. Horiz.* **2021**, *8*, 2709−2716.

(47) Quirk, J. A.; McKenna, K. P. Small-polaron mediated recombination in titanium dioxide from first principles. *Phys. Rev. Res.* **2023**, *5*, No. 023072.

(48) Kim, S.; Márquez, J. A.; Unold, T.; Walsh, A. Upper limit to the photovoltaic efficiency of imperfect crystals from first principles. *Energy Environ. Sci.* **2020**, *13*, 1481−1491.

(49) Alkauskas, A.; Yan, Q.; Van de Walle, C. G. First-principles theory of nonradiative carrier capture via multiphonon emission. *Phys. Rev. B* **2014**, *90*, No. 075202.

(50) Kim, S.; Hood, S. N.; Walsh, A. Anharmonic lattice relaxation during nonradiative carrier capture. *Phys. Rev. B* **2019**, *100*, No. 041202.

(51) Wang, X.; Kavanagh, S. R.; Scanlon, D. O.; Walsh, A. Upper efficiency limit of Sb_2Se_3 solar cells. *Joule* **2024**, *8*, 2105−2122.

(52) Dahan, N.; Jehl, A.; Guillemoles, J. F.; Lincot, D.; Naghavi, N.; Greffet, J.-J. Using radiative transfer equation to model absorption by thin Cu(In,Ga)Se_2 solar cells with lambertian back reflector. *Opt. Express* **2013**, *21*, 2563−2580.

(53) Kim, S.; Walsh, A. Ab initio calculation of the detailed balance limit to the photovoltaic efficiency of single p−n junction kesterite solar cells. *Appl. Phys. Lett.* **2021**, *118*, 243905.

(54) Kavanagh, S. R.; Walsh, A.; Scanlon, D. O. Rapid recombination by cadmium vacancies in CdTe. *ACS Energy Lett.* **2021**, *6*, 1392−1398.

(55) Nicolson, A.; Kavanagh, S. R.; Savory, C. N.; Watson, G. W.; Scanlon, D. O. Cu_2SiSe_3 as a promising solar absorber: harnessing cation dissimilarity to avoid killer antisites. *J. Mater. Chem. A* **2023**, *11*, 14833−14839.

(56) Dai, W.-W.; Zhao, Z.-Y. Defect physics of BiOI as high efficient photocatalyst driven by visible light. *J. Am. Ceram. Soc.* **2016**, *99*, 3015−3024.

(57) Sfaelou, S.; Raptis, D.; Dracopoulos, V.; Lianos, P. BiOI solar cells. *RSC Adv.* **2015**, *5*, 95813−95816.

(58) Feeney, T.; Aygur, G.; Nguyen, T.; Farooq, S.; Mendes, J.; Tuohey, H.; Gómez, D. E.; Della Gaspera, E.; van Embden, J. Solution processed bismuth oxyiodide (BiOI) thin films and solar cells. *Nanotechnology* **2023**, *34*, 305404.

(59) Blöchl, P. E. Projector augmented-wave method. *Phys. Rev. B* **1994**, *50*, 17953−17979.